

Structure and dielectric properties of $\text{Ba}_2\text{Cu}_x\text{Y}_{1-x}\text{TaO}_{6-y}$ double perovskite

F. S. Oliveira^{1*}, C. A. M. dos Santos¹, A. J. S. Machado¹, P. Banerjee² and A. Franco Jr.³

¹*Escola de Engenharia de Lorena, Universidade de São Paulo, Lorena, Brazil**

²*Department of Physics, Gandhi Institute of Technology and Management (GITAM) University, Bengaluru, India and*

³*Instituto de Física, Universidade Federal de Goiás, Goiania, Brazil*

Abstract

In this paper, we reported the effect of Cu doping on the structural and dielectric properties of $\text{Ba}_2\text{Y}_{1-x}\text{Cu}_x\text{TaO}_{6-y}$ ($0.00 \leq x \leq 0.50$) ceramics at room temperature. The Copper for Yttrium substitution reduces the sintering temperature and leads to structural changes in the Ba_2YTaO_6 rock-salt crystalline structure. Dielectric permittivity and complex impedance spectroscopy measurements suggested enhancement of the dielectric constant and occurrence of interfacial Maxwell-Wagner polarization.

arXiv:1901.05548v2 [cond-mat.mtrl-sci] 24 Oct 2019

* fso@usp.br

I. INTRODUCTION

Systematic analysis of $\text{YBa}_2\text{Cu}_3\text{O}_{7-\delta}$ (Y123) superconductor shows that Ta_2O_5 helps to achieve large-grains [1, 2] for the magnetic levitation and magnets applications [3–5]. The grain growth is attributed to the decrease in the peritectic temperature transformation [2], and the homogeneous segregation of Ba_2YTaO_6 (BYT) secondary phase in the Y123 superconducting matrix acts as vortex pinning centers, which are non-superconducting regions that confine the quantum magnetic flux, and consequently, optimizes the critical current density parameter [1, 6]. Furthermore, BYT phase also induces an unusual Paramagnetic Meissner Effect in Y123 superconductor [7].

Single Crystals of BYT were grown by Galasso *et al.* using B_2O_3 flux in 1960's [8]. Later the dielectric properties of BYT ceramic were studied in the microwave frequency range [9], and a structural phase transition [10] from cubic to tetragonal space group around 260 K was observed by diffractometry, calorimetry, transmission electronic microscopy, and Raman scattering [9, 11, 12]. This transition is quite similar to the SrTiO_3 antiferrodistortive case [13].

BYT belongs to the family of complex perovskite [14] oxides. This family group has attracted a lot of attention due to the presence of a large number of oxide materials which can be formed [15]. The long-range order of the crystal lattice are responsible for several properties in these complex perovskites [14, 15] such as the high dielectric permittivity [16, 17]. On the other hand the extrinsic giant dielectric permittivity frequency observed in related perovskites such as $\text{CaCu}_3\text{Ti}_4\text{O}_{12}$ (CCTO) [18] is a consequence of semiconducting grains limited by insulating grain boundaries which act as a kind of barrier to the free carriers motion inside the grains [19–21]. The dielectric relaxation at these barriers of charge is well described by the Maxwell-Wagner (M-W) polarization model [22–24].

Since as BYT appears as a secondary phase in Ta-doped Y123 [1], it suggests to one that Copper should have some solubility in the BYT complex perovskite, such as the $\text{Ba}_2\text{Y}_{1-x}\text{Cu}_x\text{WO}_{6-y}$ system already reported [25]. This paper presents the first investigation of the physical properties of $\text{Ba}_2\text{Y}_{1-x}\text{Cu}_x\text{TaO}_{6-y}$ system for $0.00 \leq x \leq 0.50$. Our results demonstrate that the sintering process, crystal structure, and dielectric relaxation change are dependent of the sample composition. We also show that Copper enhances the dielectric constant of BYT ceramics and leads to interfacial Maxwell-Wagner polarization at the grain boundaries. The extrinsic effects induced by Cu turns $\text{Ba}_2\text{Y}_{1-x}\text{Cu}_x\text{TaO}_{6-y}$ ceramics new candidates for some applications in electronic devices.

II. EXPERIMENTAL PROCEDURE

Ceramics of $\text{Ba}_2\text{Y}_{1-x}\text{Cu}_x\text{TaO}_{6-y}$ ($0.00 \leq x \leq 0.50$) were prepared by the standard solid state reaction method using BaCO_3 (Sigma-Aldrich, 99.95%) Y_2O_3 (Sigma-Aldrich, 99.99%) Ta_2O_5 (Cerac, 99.99%) and CuO (Sigma-Aldrich, 99.99%) powders. For each stoichiometry, powders were ball milled for about 12 hours, then calcined at 950°C in the air during 96 hours. Approximately 10% in mass of polyvinyl alcohol (PVA) binder additive was added to the powders, and disc pellets with about 8 mm in diameter and 2 mm in thickness were pressed uniaxially. These pellets were annealed at 500°C for 1 hour to decompose the organic PVA [26], and thereafter sintered in air at 1250°C to 1400°C for up to 120 hours. The microstructure of ceramics were analyzed by Scanning electron microscopy (SEM).

The crystalline structure of all samples was analyzed by XRD technique using Empirian Pan Analytical diffractometer with $\text{CuK}\alpha$ radiation ($\lambda = 1.5406 \text{ \AA}$) and Ni filter. The diffractometry measurements were carried out with 0.01° step in $10^\circ \leq 2\theta \leq 90^\circ$ range. Model refinement profiles with Pseudo-Voigt function by Rietveld method were performed in HiScore Plus program using information from inorganic crystal structure database (ICSD) [27]. Both subdomain size and microstrain were obtained from Williamson-Hall plots [28–30]. The dielectric properties of the ceramic samples were studied using a computer controlled Agilent 4980A LCR meter. An alternating voltage of 1.0 V was applied on the ceramic pellets with silver painted faces over 20 Hz to 2 MHz frequency. Nyquist plots were analyzed using EIS Spectrum Analyzer Program [31].

III. RESULTS AND DISCUSSION

The pure Ba_2YTaO_6 was formed only after long sintering time, 120 hours at 1400°C while the Cu-doped $\text{Ba}_2\text{Y}_{1-x}\text{Cu}_x\text{TaO}_{6-y}$ ($x=0.40$) was formed after much shorter sintering time, 15 hours at 1250°C . Thus it was evident that Cu for Y substitution lower both sintering temperature and sintering time. The figure 1 shows that $x = 0.40$ sample (fig. 1(b)) has signatures of liquid phase and more defects when compared with $x = 0.00$ sample (fig. 1(a)). It is an evidence that the Cu concentration contributes significantly to the microstructure.

Figure 2 exhibits the XRD patterns for $x = 0.00$ and $x = 0.50$ samples. Our analysis suggest that the sample with the highest Cu doping level possesses a single cubic perovskite crystallographic phase. The lattice parameter of the undoped sample is in good agreement with those reported in the literature [8, 9, 11, 12] and the decrease in the lattice

parameter (see inset of the figure 2(b) can be attributed to the differences in the ionic radii of Cu^{2+} (0.73 Å) and Y^{3+} (0.9 Å) ions [32].

The Williamson-Hall plot shown in Figure 3 gives the strain and the sub-cell domain information from the slope and the reciprocal of the intercept respectively [28]. The Rietveld refinement results obtained for all samples are shown in the Table I. The Cu for Y substitution produce compensating oxygen vacancies may induce strain in the crystal lattice. Additionally, XRD refinement also suggests that substitution increases the crystallite size in $\text{Ba}_2\text{Y}_{1-x}\text{Cu}_x\text{TaO}_{6-y}$ system.

In a double perovskite, the quantity of the long-range ordering degree (η) is given by [33]:

$$\eta = 2 |M_0 - 0.5| \quad (1)$$

where M_0 is the refined occupation of Ta in the 4a (0,0,0) site or the refined occupation of Y or Cu in the 4b (1/2,1/2,1/2) site [28]. Beyond that, superlattice reflection peaks are sharper in high-ordered perovskites and the ordering degree is also related to the ratio between superlattice (odd,odd,odd) and sub-cell (even,even,even) peaks of the XRD pattern [33]. The results based upon both structure refinement and peak intensities of the XRD pattern suggest that the Cu for Y substitution may reduces the long-range ordering in BYT crystalline structure, as is shown in both Table I and Figure 4.

The high dielectric permittivity observed in non-ordered double perovskites is understood in terms of randomic cation/valence long-range order distribution [14], [16]. In the $\text{Ba}_2\text{Y}_{1-x}\text{Cu}_x\text{TaO}_{6-y}$ system reported here the ordering degree decreasing affects the distribution of both compensating oxygen vacancies and hole carriers within the grains [19]. It also offers considerable contributions for the dielectric relaxation [34–37].

Figure 5(a) shows the frequency dependence of real part of permittivity (ϵ') for $\text{Ba}_2\text{Y}_{1-x}\text{Cu}_x\text{TaO}_{6-y}$. It is evident that the low frequency dielectric permittivity value for $x = 0.40$ ceramics at room temperature is higher than for $x = 0.00$. The initial high value of the real part of the dielectric permittivity could be due to the drop of applied voltage across the thin grain boundary widths and space charge polarization is generated in $x = 0.40$ and $x = 0.50$ samples, which enhances the dielectric constant at the lower frequency region.

The initial high value of dielectric constant in Cu-doped samples indicates the presence of dc conductivity due to Maxwell-Wagner (M-W) relaxation process [23], which can be better visualized in the imaginary part (ϵ'') of the dielectric permittivity shown in Figure 5b. In accordance with Maxwell-Wagner (M-W) model, the imaginary part of dielectric permittivity can be written with the following expression [24],

$$\epsilon'' = \frac{1}{\omega C_0 (R_1 + R_2)} + \Delta\epsilon' \frac{\omega\tau}{1 + \omega^2\tau^2}, \quad (2)$$

where $\sigma = 1/C_0 (R_1 + R_2)$ term is known as Ohmic conductivity (σ), where C_0 is a geometric factor, and R_1 and R_2 are the resistances of the real and imaginary dielectric components, respectively [23, 24]. The magnitude of the Ohmic conductivity can be determined from the slope of ϵ'' vs. $1/\omega$ graph, as is shown in the Figure 5(b) inset where one can see that $x = 0.40$ has the higher conductivity. The eq. 2 fits well with the experimental data which indicates the presence of M-W polarization. Hence, the oxygen vacancies generated due to the doping with Cu replacing Y increased the ohmic conductivity for $x=0.40$ and $x=0.50$ samples as they diffused into the grain boundary regions, which enhances their dielectric constants at lower frequencies.

To understand the contribution of the interfacial polarization, complex impedance spectroscopy (CIS) was performed at room temperature. The phase angle of samples is shown in figure 6(a).

In general, the approach of phase angle towards 90° represents the ideal poling state [38]. So it can be observed that slight addition of Cu enhances the poling condition $\sim 87^\circ$ in the $x = 0.10$ ceramic samples. But the magnitude of phase angle for $x = 0.40$ was found to be $\sim 76^\circ$. It suggests that sufficient amount of Cu in the Y site of Ba_2YTaO_6 crystalline structure leads to changes in poling state and domain switching.

The dependence of the impedance with frequency is shown in figure 6(b) on a double logarithmic scale. It can be observed that the magnitude of Z' decreases gradually for $x = 0.10$, $x = 0.20$, and $x = 0.30$ ceramics with the increase of ac frequency [39]. But for $x = 0.00$, $x = 0.40$, and $x = 0.50$ ceramics the magnitude of $|Z|$ decreases gradually after 10 kHz frequency. The decrease of the real part of impedance at higher frequency domain and thereafter gradual merger suggests a possible release of space charge [40] from the ceramics.

Figure 7(a) shows the Nyquist plots for $\text{Ba}_2\text{Y}_{1-x}\text{Cu}_x\text{TaO}_{6-y}$ ceramics. Since the observed semi circles are non-centered, Non-Debye type relaxation i.e. Maxwell-Wagner relaxation exists in these ceramics due to M-W relaxation [41].

An equivalent circuit shown in figure 7(b) may be represented by a bulk resistance (R_b) in series with a grain boundary resistance (R_{gb}), grain boundary capacitance (C_{gb}), and a constant phase element impedance (Z_{CPE}) in

parallel as:

$$Z(\omega) = R_b + \left[\frac{1}{R_{gb}} + \frac{1}{C_{gb}(j\omega)} + \frac{1}{P(j\omega)^n} \right]^{-1} \quad (3)$$

In, $Z_{CPE} = 1/P(j\omega)^n$, P is the CPE parameter and n is the CPE element which behaves like a double layer capacitor. The CPE is identical to a capacitance when n=1 and to a simple resistance when n=0 [42]. The experimental data fitted well with Equation 3, establishing the validity of the equivalent circuit model. The single semicircle for each type of composition indicates the single conductivity mechanism in the ceramics. Table II shows the values of the fitting parameters for the ceramics samples.

It can be observed from the magnitude of Table II that all samples the CPE behaving like a parallel capacitor-resistor in the equivalent circuit [35]. With the addition of Cu in $Ba_2Y_{1-x}Cu_xTaO_{6-y}$ both resistance and capacitance of grain boundaries increase gradually which contribute to the barrier to the motion of charge carriers within large domain bulks of electrical resistance orders of magnitude lower than the boundaries resistance. Then, we conclude that it builds up a space charge polarization across the boundary regions which was represented by M-W model.

IV. CONCLUSIONS

Ceramics samples of $Ba_2Y_{1-x}Cu_xTaO_{6-y}$ with $0.00 \leq x \leq 0.50$ were studied by X ray diffratometry, electronic scanning microscopy, dielectric permittivity measurements, and complex impedance spectroscopy. SEM images show liquid phase and defects induced by Copper. The Rietveld refinement of the XRD patterns reveal systematic changes in the crystalline structure, ordering degree, and domain sizes with the Cu content. The complex dielectric permittivity measurement demonstrated that the dielectric relaxation of $Ba_2Y_{1-x}Cu_xTaO_{6-y}$ ceramics is described by the Maxwell-Wagner model. The complex impedance spectroscopy suggests that sufficient Cu for Y substitution in Ba_2YTaO_6 ceramics leads to changes in poling state and domain switching. The study also confirmed that the x value ($0.00 \leq x \leq 0.50$) in $Ba_2Y_{1-x}Cu_xTaO_{6-y}$ ceramics affected resistance and capacitance of grain boundaries which contributed to the barrier in motion of charge and build up a space charge polarization across the boundary regions.

ACKNOWLEDGMENTS

F. S. Oliveira acknowledges the Coordenação de Aperfeiçoamento de Pessoal de Nível Superior (CAPES) - finance Code 001. P. Banerjee acknowledges UGC, India for grant no. F.30-457/2018 (BSR).

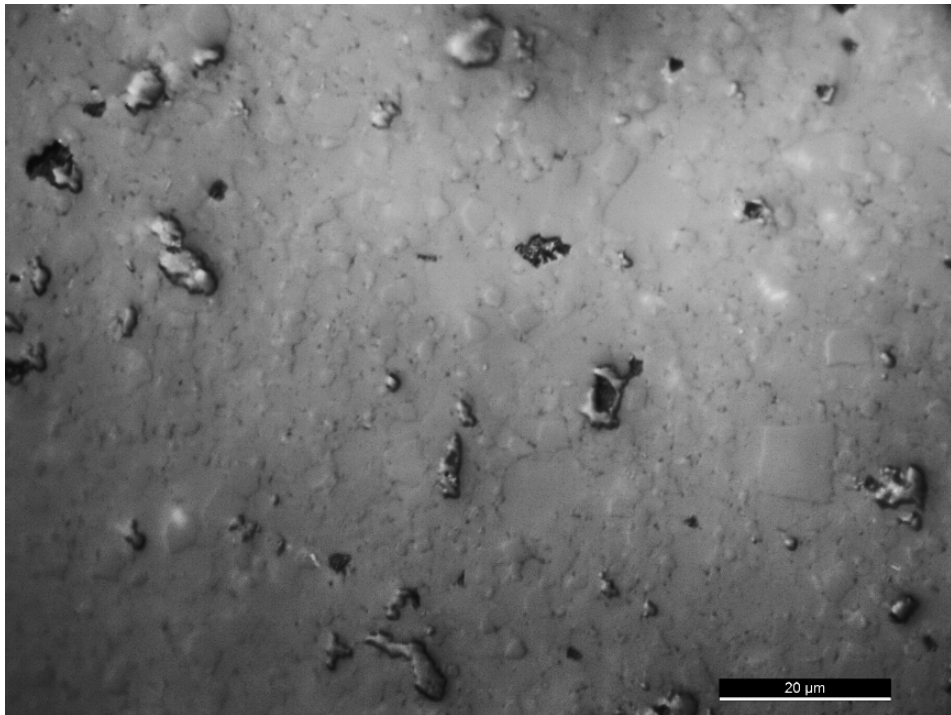
COMPLIANCE WITH ETHICAL STANDARDS

Conflict of Interest: The authors declare that they have no conflict of interest.

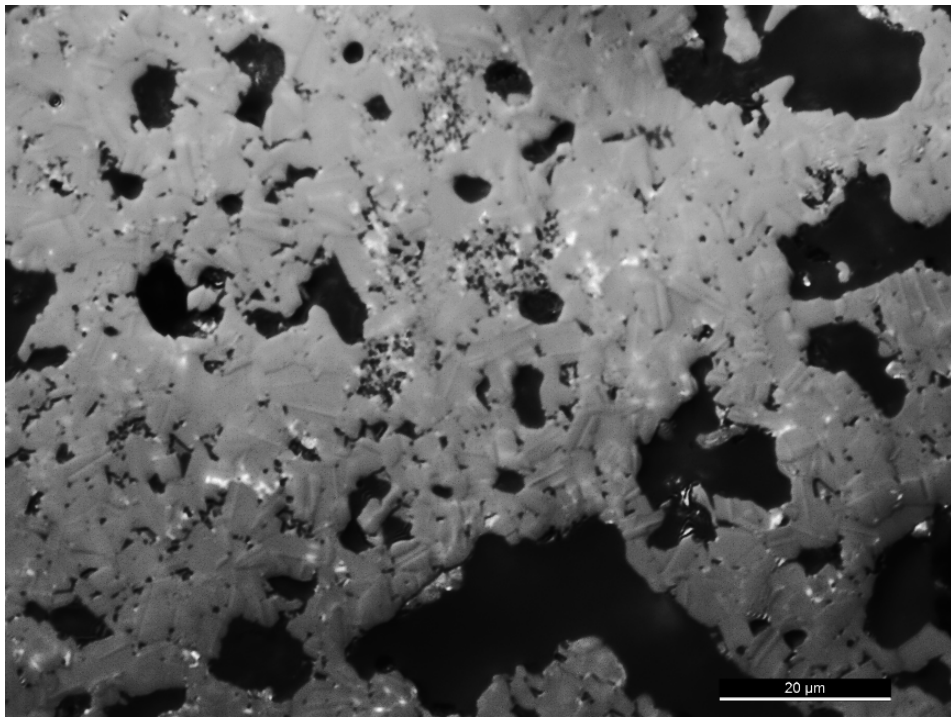
-
- [1] C J V Oliveira, A D Bortolozzo, B Ferreira, C A M dos Santos, and A J S Machado. Effect of ta₂o₅ addition on the texture of the y123 superconductor. *Physica C: Superconductivity*, 422(3-4):83–87, 2005.
 - [2] A D Bortolozzo, B Ferreira, C A M dos Santos, M A Neves, and A J S Machado. Influence of the ta doping on the peritectic transformation of ybacuo superconductor. *Physica C: Superconductivity*, 408:876–878, 2004.
 - [3] S I Bondarenko, V P Koverya, A V Krevsun, and S I Link. High-temperature superconductors of the family (re)ba₂cu₃o_{7-δ} and their application. *Low Temperature Physics*, 43(10):1125–1151, 2017.
 - [4] S O Siems, W R Canders, H Walter, and J Bock. Superconducting magnetic bearings for a 2mw/10kwh class energy storage flywheel system. *Superconductor Science and Technology*, 17(5):S229, 2004.
 - [5] R Yu, J Mora, N Vilalta, F Sandiumenge, V Gomis, S Piñol, and X Obradors. Effect of melt-processing temperature on the microstructure and the levitation force of ybco melt-textured superconductors. *Superconductor Science and Technology*, 10(8):583, 1997.
 - [6] M Coll, R Guzman, P Garcés, J Gazquez, V Rouco, A Palau, S Ye, C Magen, H Suo, H Castro, T Puig, and X Obradors. Size-controlled spontaneously segregated ba₂ytao₆ nanoparticles in yba₂cu₃o₇ nanocomposites obtained by chemical solution deposition. *Superconductor Science and Technology*, 27(4):044008, 2014.

- [7] F T Dias, V N Vieira, D L Silva, J Albino Aguiar, D R B Valadao, X Obradors, T Puig, F Wolff-Fabris, and E Kampert. Paramagnetic moments in $\text{yb}_2\text{cu}_3\text{o}_{7-\delta}$ nanocomposite films. *Physica C: Superconductivity and its Applications*, 503:175–177, 2014.
- [8] F S Galasso, G K Layden, and D E Flinchbaugh. $\text{Ba}(\text{b}_{0.5}\text{ta}_{0.5})\text{o}_3$ ordered perovskite-type compounds, possible new laser host materials. *The Journal of Chemical Physics*, 44(7):2703–2707, 1966.
- [9] R Zurmühlen, E Colla, D C Dube, J Petzelt, I Reaney, A Bell, and N Setter. Structure of $\text{ba}(\text{y}_{1/2}^{+3}\text{ta}_{1/2}^{+5})\text{o}_3$ and its dielectric properties in the range 10^2 – 10^4 hz, 20–600 k. *Journal of applied physics*, 76(10):5864–5873, 1994.
- [10] H C Karandeev, H C Gupta, and S Kumar. First principles study of structural and vibrational properties of ba_2ytao_6 in cubic and tetragonal phases. *Journal of Alloys and Compounds*, 555:335–338, 2013.
- [11] Michael W Lufaso, René B Macquart, Yongjae Lee, Thomas Vogt, and H zur Loye. Pressure induced octahedral tilting distortion in ba_2ytao_6 . *Chemical Communications*, (2):168–170, 2006.
- [12] Qingdi Zhou, Brendan J Kennedy, and Justin A Kimpton. The effect of disorder in ba_2ytao_6 on the tetragonal to cubic phase transition. *Journal of Solid State Chemistry*, 184(4):729–734, 2011.
- [13] B S de Lima, M S da Luz, F S Oliveira, L M S Alves, C A M dos Santos, F Jomard, Y Sidis, P Bourges, S Harms, C P Grams, J Hemberger, X Lin, B Faqué, and K Behnia. Interplay between antiferrodistortive, ferroelectric, and superconducting instabilities in $\text{sr}_{1-x}\text{ca}_x\text{tio}_{3-\delta}$. *Physical Review B*, 91(4):045108, 2015.
- [14] Graham King and Patrick M Woodward. Cation ordering in perovskites. *Journal of Materials Chemistry*, 20(28):5785–5796, 2010.
- [15] Sami Vasala and Maarit Karppinen. A2B B O6 perovskites: a review. *Progress in solid state chemistry*, 43(1-2):1–36, 2015.
- [16] S Yañez-Vilar, M Sánchez-Andújar, J Rivas, and M A Señarís-Rodríguez. Influence of the cationic ordering in the dielectric properties of the $\text{la}_2\text{mncoo}_6$ perovskite. *Journal of Alloys and Compounds*, 485(1-2):82–87, 2009.
- [17] K Devi Chandrasekhar, A K Das, Chiranjib Mitra, and A Venimadhav. The extrinsic origin of the magnetodielectric effect in the double perovskite $\text{la}_2\text{nimno}_6$. *Journal of Physics: Condensed Matter*, 24(49):495901, 2012.
- [18] M A Subramanian, Dong Li, N Duan, B A Reisner, and A W Sleight. High dielectric constant in $\text{acu}_3\text{ti}_4\text{o}_{12}$ and $\text{acu}_3\text{ti}_3\text{feo}_{12}$ phases. *Journal of Solid State Chemistry*, 151(2):323–325, 2000.
- [19] Timothy B Adams, Derek C Sinclair, and Anthony R West. Giant barrier layer capacitance effects in $\text{cacu}_3\text{ti}_4\text{o}_{12}$ ceramics. *Advanced Materials*, 14(18):1321–1323, 2002.
- [20] T Y Tien and L E Cross. Dielectric relaxation in strontium titanate solid solutions containing lanthania. *Japanese Journal of Applied Physics*, 6(4):459, 1967.
- [21] Rainer Waser. Bulk conductivity and defect chemistry of acceptor-doped strontium titanate in the quenched state. *Journal of the American Ceramic Society*, 74(8):1934–1940, 1991.
- [22] Guojing Wang, Chunchang Wang, Shouguo Huang, Changmei Lei, Xiaohong Sun, Teng Li, and Lina Liu. Origin of colossal dielectric behavior in double perovskite $\text{ba}_2\text{conbo}_6$. *Journal of the American Ceramic Society*, 96(7):2203–2210, 2013.
- [23] D O Neill, R M Bowman, and J M Gregg. Dielectric enhancement and maxwell–wagner effects in ferroelectric superlattice structures. *Applied Physics Letters*, 77(10):1520–1522, 2000.
- [24] Prasun Banerjee and Adolfo Franco Jr. Substitution-induced near phase transition with maxwell–wagner polarization in $\text{srb}_2(\text{nb}_{1-x}\text{a}_x)_2\text{o}_9$ ceramics [a= w, mo and x= 0, 0.025]. *physica status solidi (a)*, 214(10):1700067, 2017.
- [25] A Garcia-Ruiz, Bokhimi, and M Portilla. Solid solutions in the $\text{ba}_2\text{y}_{1-x}\text{cu}_x\text{wo}_{6-y}$ system. *Journal of materials research*, 7(1):24–28, 1992.
- [26] P Banerjee and A Franco. Rare earth and transition metal doped bifeo₃ ceramics: Structural, magnetic and dielectric characterization. *Journal of Materials Science: Materials in Electronics*, 27(6):6053–6059, 2016.
- [27] Alec Belsky, Mariette Hellenbrandt, Vicky Lynn Karen, and Peter Luksch. New developments in the inorganic crystal structure database (icsd): accessibility in support of materials research and design. *Acta Crystallographica Section B: Structural Science*, 58(3):364–369, 2002.
- [28] P Woodward, R D Hoffmann, and A W Sleight. Order-disorder in $\text{a}_2\text{m}^{3+}\text{m}^{5+}\text{o}_6$ perovskites. *Journal of Materials Research*, 9(8):2118–2127, 1994.
- [29] T E P Alves, H V S Pessoni, and A Franco Jr. The effect of y^{3+} substitution on the structural, optical band-gap, and magnetic properties of cobalt ferrite nanoparticles. *Physical Chemistry Chemical Physics*, 19(25):16395–16405, 2017.
- [30] Ah Dhahri, E Dhahri, and E K Hlil. Electrical conductivity and dielectric behaviour of nanocrystalline $\text{la}_{0.6}\text{gd}_{0.1}\text{sr}_{0.3}\text{mn}_{0.75}\text{si}_{0.25}\text{o}_3$. *RSC Advances*, 8(17):9103–9111, 2018.
- [31] AS Bondarenko and GA Ragoisha. *Inverse problem in potentiodynamic electrochemical impedance*. Nova Science Publishers: New York, 2005.
- [32] Robert D Shannon. Revised effective ionic radii and systematic studies of interatomic distances in halides and chalcogenides. *Acta crystallographica section A: crystal physics, diffraction, theoretical and general crystallography*, 32(5):751–767, 1976.
- [33] G Y Liu, G H Rao, X M Feng, H F Yang, Z W Ouyang, W F Liu, and J K Liang. Atomic ordering and magnetic properties of non-stoichiometric double-perovskite $\text{sr}_2\text{fe}_x\text{mo}_{2-x}\text{o}_6$. *Journal of Physics: Condensed Matter*, 15(12):2053, 2003.
- [34] W Z Yang, M M Mao, X Q Liu, and X M Chen. Structure and dielectric relaxation of double-perovskite $\text{la}_2\text{cutio}_6$ ceramics. *Journal of Applied Physics*, 107(12):124102, 2010.
- [35] Dev K Mahato and T P Sinha. Dielectric, impedance and conduction behavior of double perovskite $\text{pr}_2\text{cutio}_6$ ceramics. *Journal of Electronic Materials*, 46(1):107–115, 2017.
- [36] Hari Mohan Rai, Shailendra K Saxena, Ravikiran Late, Vikash Mishra, Parasmani Rajput, Archana Sagdeo, Rajesh Kumar, and P R Sagdeo. Observation of large dielectric permittivity and dielectric relaxation phenomenon in mn-doped lanthanum

- gallate. *RSC Advances*, 6(32):26621–26629, 2016.
- [37] Raphael Lucas de Sousa e Silva, Prasun Banerjee, and Adolfo Franco Junior. Functional properties of donor-and acceptor-co-doped high dielectric constant zinc oxide ceramics. *Physical Chemistry Chemical Physics*, 21(18):9456–9464, 2019.
- [38] J L Izquierdo, G Bolanos, V H Zapata, and O Moran. Dielectric relaxation and ac conduction in multiferroic tbmno_3 ceramics: Impedance spectroscopy analysis. *Current Applied Physics*, 14(11):1492–1497, 2014.
- [39] Poonam Kumari, Radheshyam Rai, and A L Kholkin. Influence of bifetao_3 addition on the electrical properties of $\text{nao}_{0.4725}\text{ko}_{0.4725}\text{li}_{0.055}\text{nbo}_3$ ceramics system using impedance spectroscopy. *Journal of Alloys and Compounds*, 637:203–212, 2015.
- [40] B C Sutar, R N P Choudhary, and Piyush R Das. Dielectric and impedance spectroscopy of $\text{Sr}(\text{Bi}_{0.5}\text{Nb}_{0.5})\text{O}_3$ ceramics. *Ceramics International*, 40(6):7791–7798, 2014.
- [41] Yevgen Barsukov and J Ross Macdonald. Electrochemical impedance spectroscopy. *Characterization of materials*, 2:1–16, 2012.
- [42] Shenglong Yu, Hailin Bi, Jialing Sun, Lili Zhu, Huamin Yu, Chunling Lu, and Xiaomei Liu. Effect of grain size on the electrical properties of strontium and magnesium doped lanthanum gallate electrolytes. *Journal of Alloys and Compounds*, 777:244–251, 2019.

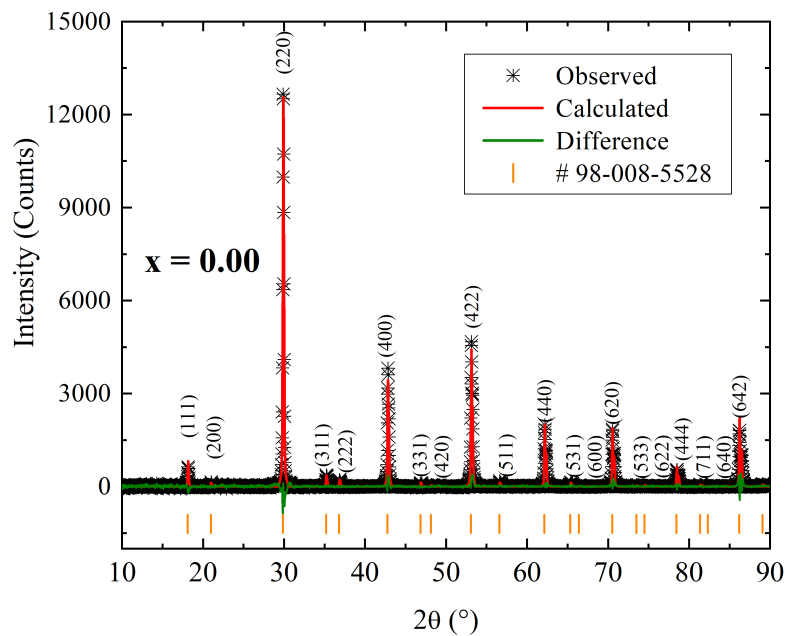


(a)

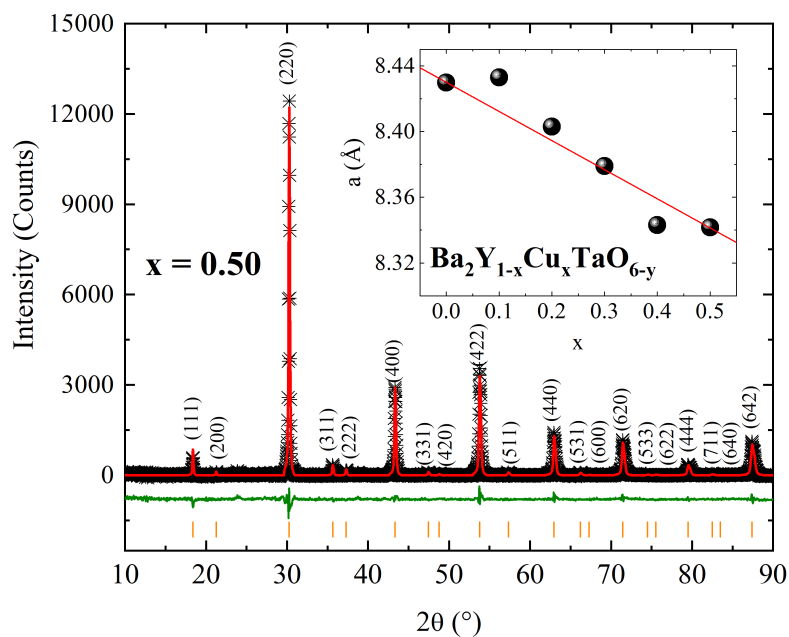


(b)

Figure 1: SEM images for (a) $x = 0.00$ and (b) $x = 0.40$ sample.



(a)



(b)

Figure 2: (a) XRD pattern of $x = 0.00$ sample sintered at 1450°C for 120 hours. (b) XRD pattern of $x = 0.50$ sample sintered at 1250°C for 15 hours. The inset shows the Vegard's law dependence between lattice parameter and copper content.

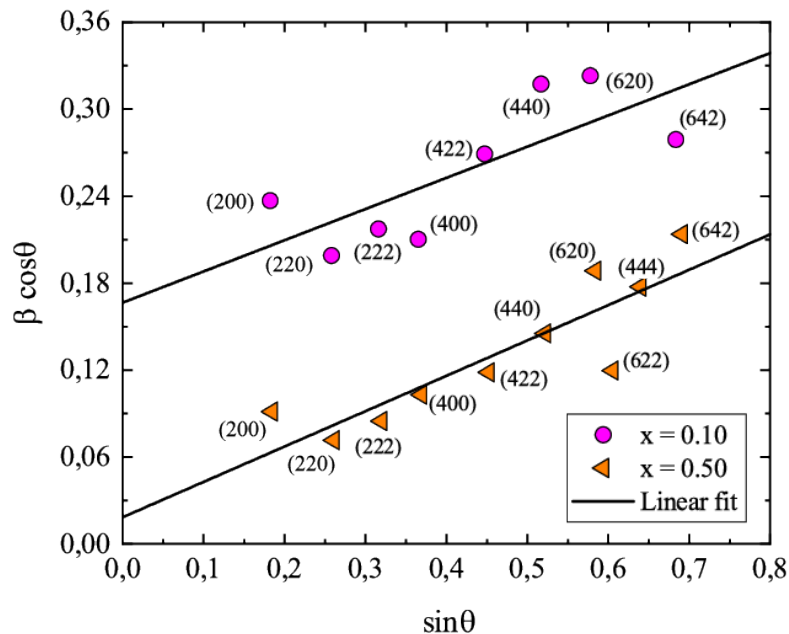


Figure 3: Williamson-Hall plot of $x = 0.10$ and $x = 0.50$, where β is the full width at half maximum of the reflection peaks.

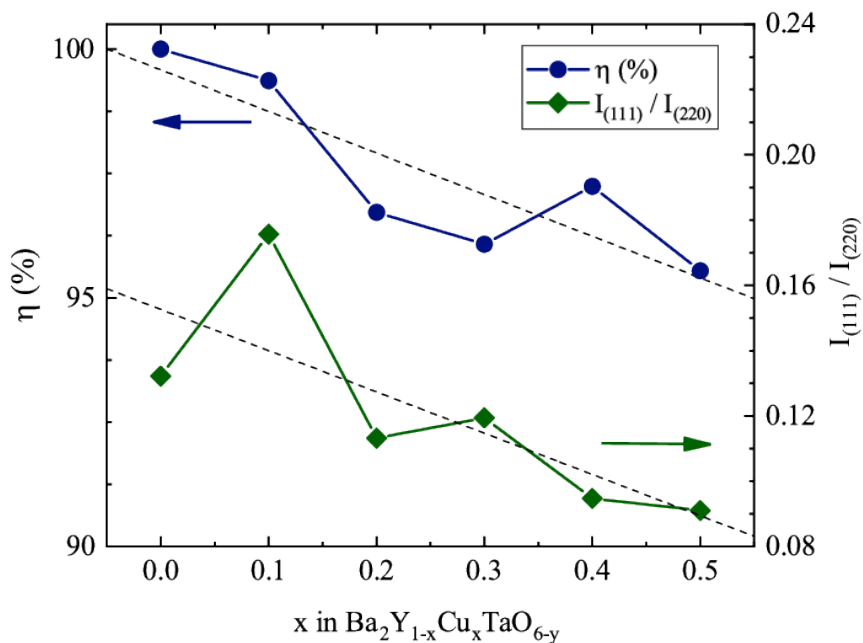


Figure 4: Ordering degree (left-axis) and ratio between (111) and (220) peak intensities (right-axis). The dashed lines are just a guides to the eyes.

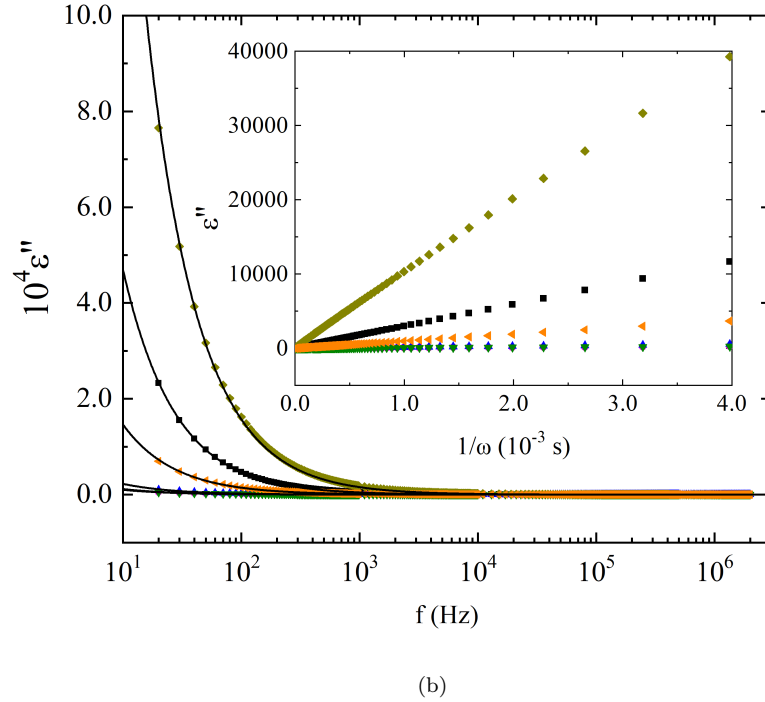
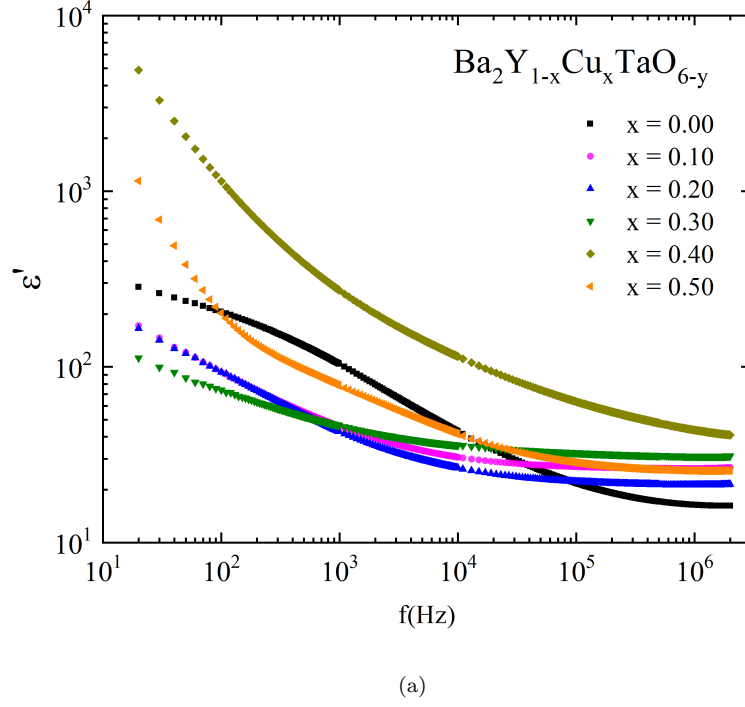


Figure 5: Variation of (a) Real (ϵ') and (b) Imaginary (ϵ'') parts of permittivity with the variation of frequency at room temperature, the solid lines shows the fitting with Maxwell-Wagner model using Equation 2 and the inset shows ϵ'' as function as $1/\omega$.

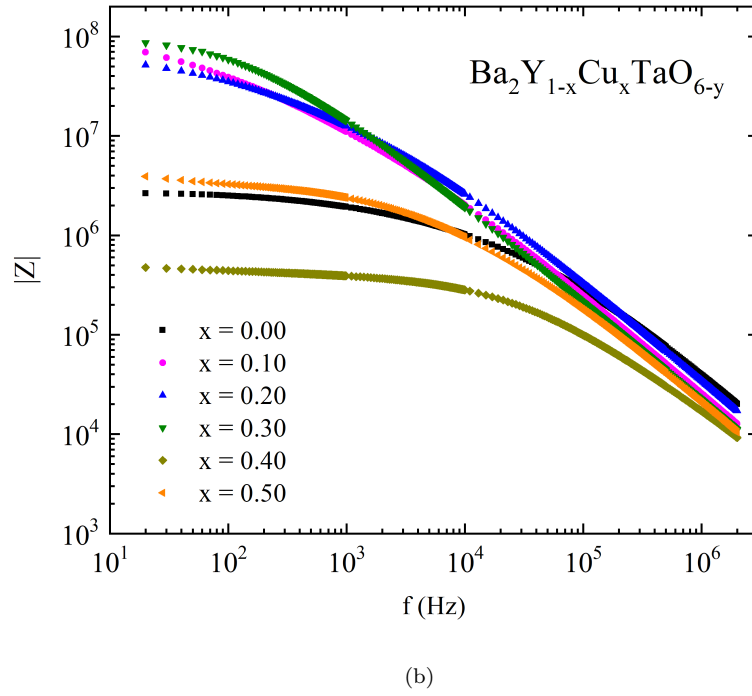
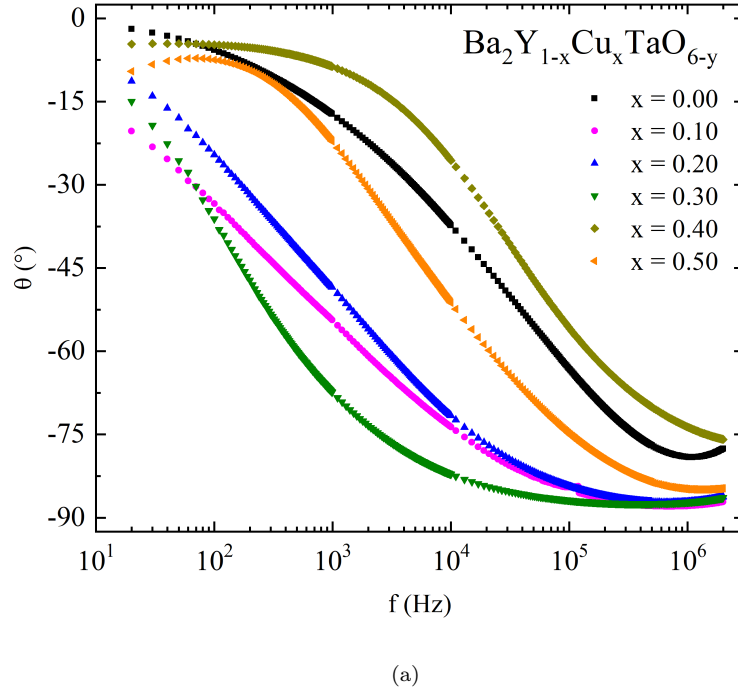


Figure 6: (a) Dependence of phase angle with frequency at room temperature and (b) Dependence of real part of impedance (Z') with frequency at room temperature.

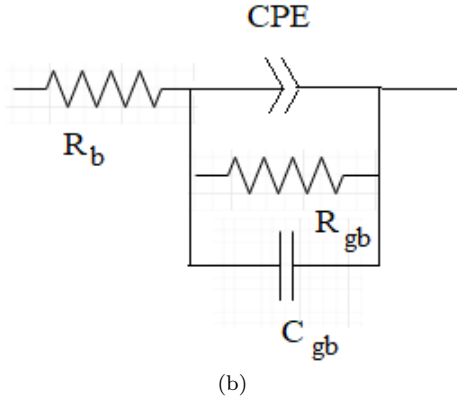
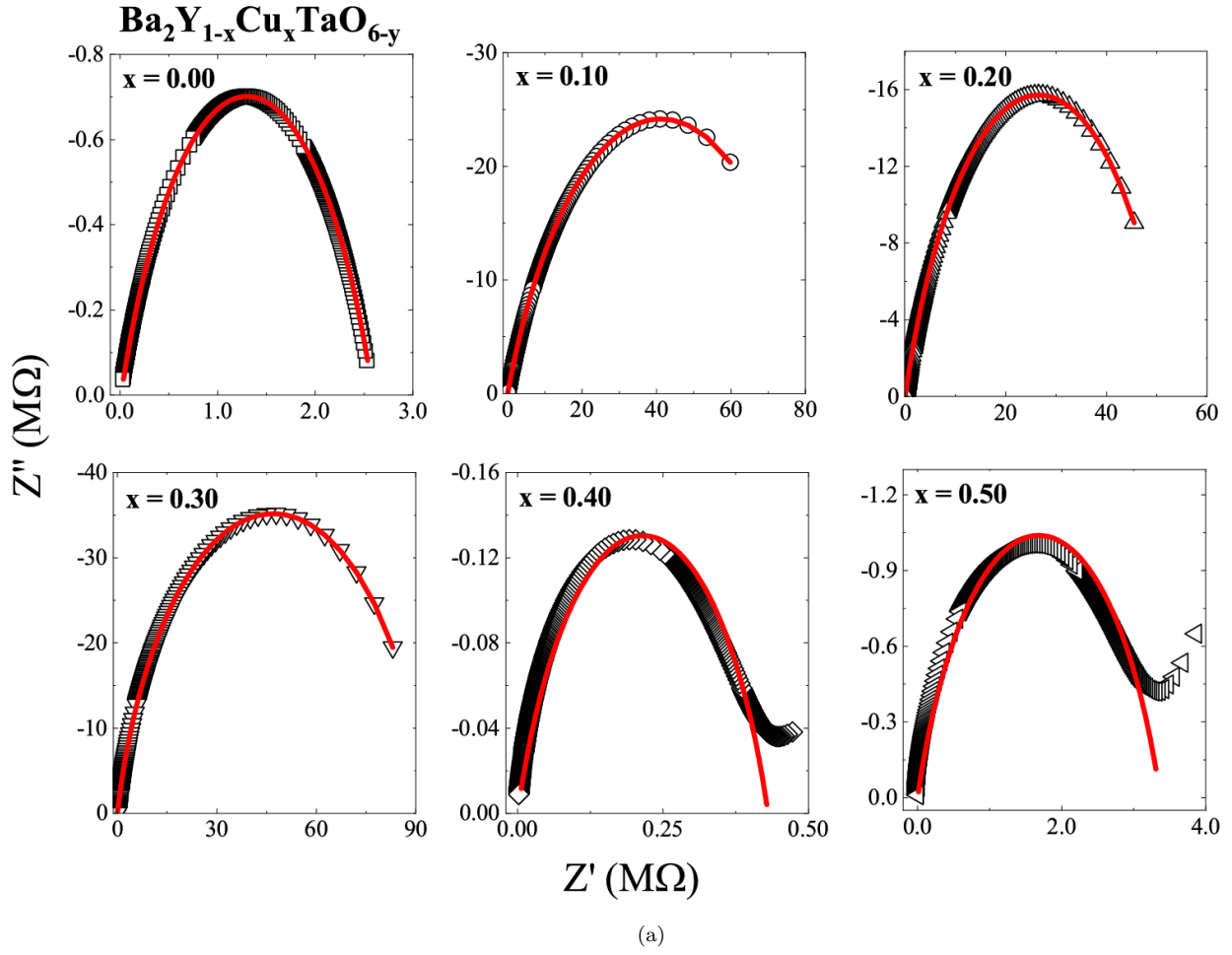


Figure 7: (a) Nyquist plots for Ba₂Y_{1-x}Cu_xTaO_{6-y} ceramics with $0.00 \leq x \leq 0.50$ (markers) and solid lines are fits using Equation 3. (b) Equivalent circuit used for fitting.

Table I: Rietveld refinement results as function as x in $\text{Ba}_2\text{Y}_{1-x}\text{Cu}_x\text{TaO}_{6-y}$. Refinement agreement factors: R_{exp} (expected) R_p (profile), R_{wp} (pondered profile), and goodness of fit (χ^2). Lattice parameter (a), crystallite size (D), strain (ϵ), ordering degree (η), and the ratio between (111) and (220) peak intensities.

	$\text{Ba}_2\text{Y}_{1-x}\text{Cu}_x\text{TaO}_{6-y}$					
x	0.00	0.10	0.20	0.30	0.40	0.50
R_{exp} (%)	5.11	5.69	5.13	6.48	4.62	5.13
R_p (%)	8.58	9.01	9.45	6.13	4.31	7.3
R_{wp} (%)	17.55	15.96	18.36	7.42	5.63	14
χ^2	3.42	2.81	3.58	1.14	1.22	2.73
a (Å)	8.423(1)	8.433(1)	8.403(1)	8.379(1)	8.343(1)	8.342(3)
D (Å)	973(229)	830(96)	1041(236)	1031(201)	4338(2590)	4795(2723)
ϵ (%)	0.05(4)	0.09(4)	0.04(2)	0.04(2)	0.09(3)	0.11(2)
η (%)	99.9	99.4	96.7	96.1	97.2	95.5
$I_{(111)} : I_{(220)}$	0.132	0.176	0.113	0.119	0.095	0.090

Table II: Electrical parameters of the equivalent electrical circuit obtained from complex impedance spectrum fits using Equation 3 for $\text{BaY}_{1-x}\text{Cu}_x\text{TaO}_{6-y}$ samples

x	R_b (kΩ)	R_{gb} (MΩ)	C_{gb} (pF)	P (nFs^{n-1})	n
0.00	4.06	2.82	3.157	2.81	0.484
0.10	263.5	92.21	3.18	0.378	0.587
0.20	63.5	58.76	2.743	0.363	0.571
0.30	71.76	10.22	6.01	0.12	0.642
0.40	4.74	0.47	9.672	12.2	0.435
0.50	12.85	3.75	7.22	2.264	0.491